PNAS RESEARCH ARTICLE | BIOCHEMISTRY

Modulation of amyloid precursor protein cleavage by γ-secretase activating protein through phase separation

Chen Jin[a], Jiaoni Wang[a], Yumeng Wang[a], Bojun Jia[a], Xuefei Guo[a], Guanghui Yang[b], Peng Xu[c], Paul Greengard[c], Rui Zhou[a,1], and Yigong Shi (施一公)[a,d,e,f,1]

Contributed by Yigong Shi; received December 9, 2021; accepted February 17, 2022; reviewed by Yueming Li, Gang Yu, and Mingjie Zhang

Aberrant cleavage of amyloid precursor protein (APP) by γ-secretase is closely associated with Alzheimer's disease (AD). γ-secretase activating protein (GSAP) specifically promotes γ-secretase–mediated cleavage of APP. However, the underlying mechanism remains enigmatic. Here, we demonstrate that the 16-kDa C-terminal fragment of GSAP (GSAP-16K) undergoes phase separation in vitro and forms puncta-like condensates in cells. GSAP-16K exerts dual modulation on γ-secretase cleavage; GSAP-16K in dilute phase increases APP–C-terminal 99-residue fragment (C99) cleavage toward preferred production of β-amyloid peptide 42 (Aβ42), but GSAP-16K condensates reduce APP-C99 cleavage through substrate sequestration. Notably, the Aβ42/Aβ40 ratio is markedly elevated with increasing concentrations of GSAP-16K. GSAP-16K stably associates with APP-C99 through specific sequence elements. These findings mechanistically explain GSAP-mediated modulation of γ-secretase activity that may have ramifications on the development of potential therapeutics.

γ-secretase | Alzheimer's disease | γ-secretase activating protein | amyloid precursor protein | liquid–liquid phase separation

Significance

γ-secretase activating protein (GSAP) has emerged as a key regulator of γ-secretase. In cells, GSAP exists primarily in the form of a 16-kDa fragment known as GSAP-16K. In this study, we report the finding that GSAP-16K undergoes phase separation in vitro and in cells. Importantly, the outcome of GSAP-16K phase separation directly regulates the protease activity of human γ-secretase. Through direct interaction with the substrate amyloid precursor protein–C-terminal 99-residue fragment, GSAP-16K in dilute phase favors the production of β-amyloid peptide 42 (Aβ42) but not Aβ40. These observations not only explain how GSAP activates γ-secretase but also identify their interaction as a target of potential therapeutic intervention.

Alzheimer's disease (AD), affecting over 40 million patients worldwide, is characterized by amyloid plaques in patient brain (1–4). Amyloid plaques are aggregates of β-amyloid peptides (Aβs), the cleavage products of the amyloid precursor protein (APP) (5). APP is first cleaved by β-secretase to generate a C-terminal 99-residue fragment (C99), which is subsequently processed by γ-secretase to generate the amyloid precursor protein intracellular domain (AICD) and Aβ of varying lengths (6–8). The intramembrane protease γ-secretase comprises APH-1, nicastrin, Pen-2, and the catalytic component presenilin (PS1/PS2) (9, 10). Reducing Aβ production through γ-secretase inhibition represents an attractive therapeutic strategy for AD treatment (11, 12). However, substrate-selective inhibition of γ-secretase is complicated by its broad range of substrates (13, 14). One strategy to overcome this hurdle is to identify new protein targets that only regulate APP cleavage.

γ-secretase activating protein (GSAP) was identified as a specific activator of APP cleavage (15, 16). The expression levels of GSAP appear to correlate with the susceptibility and severity of AD, presenting GSAP as a potential target for AD treatment (16–18). Increased GSAP levels are found in the brains of deceased AD patients (19). Decreased expression of GSAP led to reduced Aβ production in an AD mouse model (20) and in cells (16, 21, 22). In cells, the 98-kDa GSAP protein is rapidly processed into a 16-kDa C-terminal fragment (known as GSAP-16K) (16).

GSAP-16K was found to associate with both γ-secretase and APP-C99 in cell extracts (16). Although GSAP-16K directly binds AICD (23), there is no evidence for direct interactions between GSAP-16K and γ-secretase. Nonetheless, it is postulated that GSAP-16K might activate γ-secretase by inducing conformational changes in the catalytic component of PS1 (16, 21). However, this hypothesis fails to explain why such changes have no impact on other substrates of γ-secretase. At present, the mechanism by which GSAP-16K modulates γ-secretase remains largely unknown.

In this study, we demonstrate that GSAP-16K undergoes liquid–liquid phase separation (LLPS) to form puncta-like condensates/droplets in vitro and in cells. GSAP-16K in dilute phase stimulates the protease activity of γ-secretase by delivering the substrate APP-C99. Notably, the specific interaction between GSAP-16K and APP-C99 vastly favors the production of Aβ42 but not Aβ40. In its droplet/condensate form, GSAP-16K sequesters APP-C99, making it inaccessible to γ-secretase and thus, decreasing the protease activity. Together, as a result of phase separation, increasing concentrations of GSAP-16K lead to a bell-shaped curve of γ-secretase activity but steadily increasing Aβ42/Aβ40 ratios.

Author contributions: C.J., J.W., Y.W., B.J., X.G., G.Y., P.X., P.G., R.Z., and Y.S. designed research; C.J., J.W., Y.W., B.J., X.G., G.Y., and R.Z. performed research; C.J., G.Y., R.Z., and Y.S. analyzed data; and C.J., R.Z., and Y.S. wrote the paper.

Reviewers: Y.L., Memorial Sloan Kettering Cancer Center; G.Y., University of Texas Southwestern Medical Center; and M.Z., Southern University of Science and Technology.

The authors declare no competing interest.

[1]To whom correspondence may be addressed. Email: ruizhou1223@163.com or syg@westlake.edu.cn.

This article contains supporting information online at http://www.pnas.org/lookup/suppl/doi:10.1073/pnas.2122292119/-/DCSupplemental.

Published March 17, 2022.

Results

GSAP-16K Undergoes LLPS In Vitro. To investigate the modulation of γ-secretase by GSAP-16K, we sought to express and purify GSAP-16K. As previously observed (23, 24), recombinant GSAP-16K exhibits a strong tendency to self-associate into inclusion bodies in *Escherichia coli*. To break up the self-association, we purified GSAP-16K in the presence of the detergent empigen (24). With Fos-Choline-12 (FC12) in the buffer, the gel filtration peak for GSAP-16K is symmetric (*SI Appendix*, Fig. S1*A*), suggesting monodispersity. Notably, once the detergent FC12 is removed, the purified GSAP-16K is prone to aggregation and precipitation. It is likely that GSAP-16K oligomerizes in the aggregated and/or precipitated states. The purified GSAP-16K protein displays clear features of α-helices as judged by circular dichroism (CD) measurements over a range of temperatures (*SI Appendix*, Fig. S1*B*). Analysis of the CD spectra reveals a melting temperature of about 80 °C for GSAP-16K (*SI Appendix*, Fig. S1*C*). Consistent with these analyses, GSAP-16K contains a stable structural core that is resistant to limited proteolysis (*SI Appendix*, Fig. S1*D*).

During the process of characterizing recombinant GSAP-16K, we serendipitously discovered its phase separation. To systematically investigate this phenomenon, we conjugated the purified GSAP-16K protein to the fluorescent dye Alexa647. In the presence of 10% polyethylene glycol (PEG) of varying molecular mass, the solution state of the labeled GSAP-16K at 10 μM concentration was examined using a laser scanning confocal microscope (Fig. 1*A*). Under the condition of no PEG or low–molecular mass PEG, GSAP-16K appeared to form liquid droplets, which occupy less than 0.1% of the total area. In contrast, the presence of PEG8000 allowed formation of more prominent liquid droplets that occupy about 1.8% of the total area (Fig. 1*A* and *SI Appendix*, Fig. S2*A*).

Protein concentration and ionic strength are known to influence LLPS (25, 26). We examined the ability of GSAP-16K over five different concentrations to form droplets under five distinct ionic strengths as measured by NaCl concentration (Fig. 1*B*). Consistent with previous knowledge (26), high concentrations of GSAP-16K (equal to or above 20 μM) and low concentrations of NaCl (equal to or below 150 mM) engender formation of obvious droplets that occupy at least 7.1% of the total area (Fig. 1*B* and *SI Appendix*, Fig. S2*B*). In contrast, lower concentrations of GSAP-16K (equal to or below 10 μM) or higher concentrations of NaCl (equal to or above 300 mM) give rise to droplets that occupy no more than 1.5% of the total area (Fig. 1*B* and *SI Appendix*, Fig. S2*B*). These results demonstrate that formation of the GSAP-16K droplets is susceptible to high ionic strength (equal to or above 300 mM NaCl).

The fluidic nature of these droplets is demonstrated by the fusion of two droplets into a larger one over the course of 60 min (Fig. 1*C* and Movie S1). We further examined the fluidity of the droplets by observing fluorescence recovery after photobleaching (FRAP). Immediately after photobleaching (0 min), the fluorescence signal of the GSAP-16K droplet was reduced to about 20% of its original value prior to photobleaching (Fig. 1*D*). The signal recovered steadily, reaching about 55% of the original value after 15 min. Notably, the rates of fusion and fluorescence recovery of the GSAP-16K droplets are slower than those of classic LLPS, where such processes usually occur within several minutes (27–31).

All above experiments were performed in the presence of PEG8000 because high–molecular mass PEG is known to facilitate LLPS (26, 32). In the absence of PEG8000, GSAP-16K also undergoes LLPS, except that the area occupied by the droplets is less than 2% of the total area (Fig. 1*E* and *SI Appendix*, Fig. S2*C*). Compared with those in the presence of PEG8000, the size and number of these droplets are more susceptible to high ionic strength. With 300 mM NaCl, the droplets formed by 40 μM GSAP-16K occupy less than 0.05% of the total area (Fig. 1*E* and *SI Appendix*, Fig. S2*C*).

GSAP-16K Forms Puncta-Like Condensates/Droplets in Cells. To investigate whether GSAP-16K also undergoes LLPS in cells, we generated two HEK293FT cell lines, one stably expressing GSAP-16K with an N-terminal GFP (GFP-GSAP-16K) and the other expressing GFP alone. The two cell lines were validated by amplifying the specific sequences from genomic DNA (*SI Appendix*, Fig. S3*A*) and immunoblotting the cell lysates with an anti-GFP monoclonal antibody (*SI Appendix*, Fig. S3*B*). Puncta-like condensates and droplets were observed in the cells that stably expressed GFP-GSAP-16K but not GFP alone (*SI Appendix*, Fig. S3*C*). Statistical analysis reveals the presence of puncta in 24 ± 3% of all cells. Each cell contains ∼33 ± 14 puncta-like condensates, which occupy 15 ± 5% of the total cellular area (*SI Appendix*, Fig. S3*D*).

These puncta-like condensates and droplets display clear features of fluidity. Within the HEK293FT cell, two small droplets formed by GFP-GSAP-16K were fused into a larger droplet within 10 s (Fig. 2*A* and Movie S2). The droplet fusion in cells is at least two orders of magnitude faster than that in solution (Fig. 1*C*). The highly mobile nature of these small GFP-GSAP-16K droplets in cells makes the FRAP experiment technically challenging. Nonetheless, we succeeded in photobleaching a few slightly larger droplets. Within the course of about 30 s, the averaged fluorescence signal of the photobleached droplet had been recovered from 17 to 33% of the original value (Fig. 2*B*).

Next, we examined whether endogenous GSAP also undergoes LLPS in cells. Once translated, the full-length GSAP is processed to yield GSAP-16K within 2 h (16). Using an anti–GSAP-16K antibody, we stained cortical cells from a postnatal day 0 (P0) mouse (Fig. 2*C*). The cells were also stained by Hoechst33258 for nuclei and by an anti-Tuj1 antibody for their neuronal origin (Fig. 2*C*). Consistent with a previous study (16), GSAP-16K is localized exclusively in the cytoplasm. Puncta-like condensates and small droplets are clearly seen among the diffuse staining pattern of endogenous GSAP-16K (Fig. 2*C*). In contrast, immunostaining of the cortical cells using an antibody against the N terminus of GSAP results in a mostly diffuse staining pattern (*SI Appendix*, Fig. S3*E*). Compared with cells stained by the antibody against the C terminus of GSAP, the average number of puncta-like condensates in cells stained by the antibody against the N terminus of GSAP is at least 10-fold less (*SI Appendix*, Fig. S3*F*). Therefore, GSAP-16K, rather than the full-length GSAP, makes a predominant contribution to puncta formation in mouse cortical neuron cells.

Incorporation of AICD into GSAP-16K Condensates/Droplets. GSAP-16K was reported to associate with AICD in vitro and in cells (16, 23). Because GSAP-16K undergoes LLPS, we examined whether AICD could be incorporated into these condensates/droplets. GSAP-16K (*SI Appendix*, Fig. S1*A*) and AICD with an N-terminal GST (GST-AICD) (*SI Appendix*, Fig. S4*A*) were individually purified to homogeneity and labeled with the fluorescent dyes Alexa647 and Alexa488,

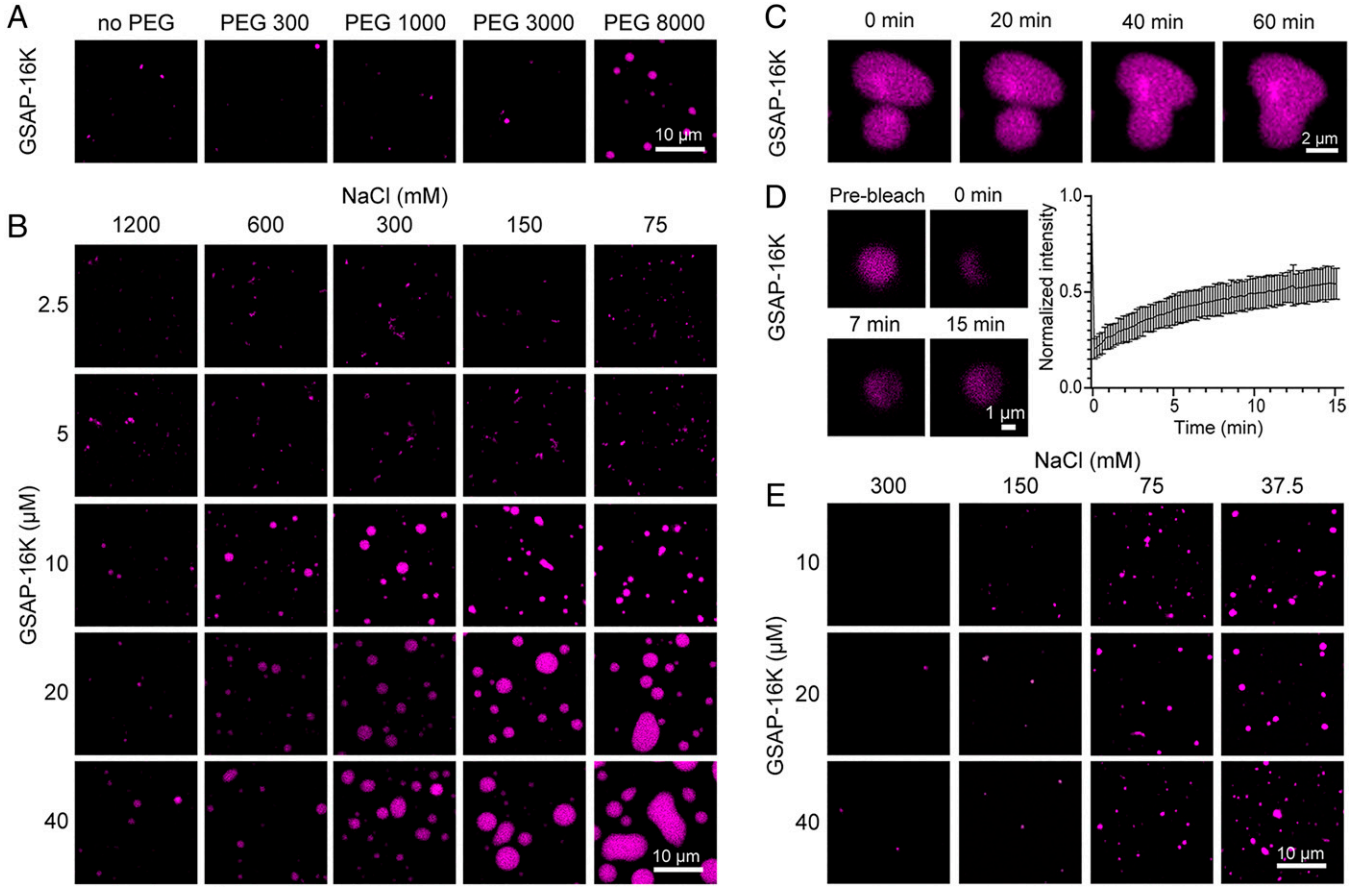

Fig. 1. GSAP-16K undergoes LLPS in vitro. (*A*) Recombinant GSAP-16K protein forms droplets preferentially in the presence of high-molecular mass PEG. GSAP-16K at 10 μM was incubated with 10% (wt/vol) PEG of varying molecular mass. All images in this study were taken using a confocal laser scanning microscope unless otherwise stated. (*B*) Higher concentrations of GSAP-16K and lower ionic strengths favor droplet formation. Five concentrations of GSAP-16 were evaluated for droplet formation under five distinct ionic strengths in the presence of 10% (wt/vol) PEG8000. (*C*) Fusion of two neighboring GSAP-16K droplets. GSAP-16K at 10 μM was monitored in the presence of 10% PEG 8000. (*D*) The GSAP-16K droplets show FRAP. Four temporal snapshots of a representative GSAP-16K droplet are shown in *Left*. Quantitative analysis, averaged for the results of FRAP on three different droplets, is shown in *Right*. Error bar: SD. (*E*) Formation of GSAP-16K puncta-like condensates and droplets in the absence of PEG. Three concentrations of GSAP-16K were evaluated for LLPS under four distinct ionic strengths in the absence of PEG.

respectively. Labeled GST-AICD at varying concentrations was incubated with 40 μM labeled GSAP-16K for an hour and analyzed using confocal microscopy (Fig. 3*A*). In all cases, the target proteins form puncta-like condensates/droplets (Fig. 3*A*, first two columns).With increasing GST-AICD concentrations, the puncta-like condensates/droplets occupy increasing percentages of the total area (*SI Appendix*, Fig. S4*B*). Remarkably, for nearly all droplets, the fluorescence signals of GST-AICD coincide with those of GSAP-16K (Fig. 3*A*, third column). This finding is further validated by a line scan of the image of Alexa488-labeled GST-AICD and Alexa647-labeled GSAP-16K (*SI Appendix*, Fig. S4*C*). GST-AICD alone produced no such condensates/droplets (Fig. 3*A*, fourth column).

These results, together with the observation that GSAP-16K alone also forms droplets in vitro (Fig. 1), strongly suggest that GST-AICD is incorporated into the condensates/droplets through its interaction with GSAP-16K. To rule out the possibility that this process is mediated by GST rather than AICD, we performed a set of control experiments (Fig. 3*B*). In this case, GST and GSAP-16K were labeled with Alexa488 and Alexa647, respectively. These labeled proteins were similarly incubated and analyzed using confocal microscopy (Fig. 3*B*). GST fails to be incorporated into the GSAP-16K condensates/droplets (Fig. 3*B*).

In the above experiments (Fig. 3*A*), GSAP-16K was kept under the condition in which condensates/droplets can hardly be formed prior to incubation with GST-AICD. We examined whether GST-AICD can be incorporated into GSAP-16K droplets that have already formed. GST-AICD protein was added to a solution of preformed GSAP-16K droplets. Time-resolved imaging reveals that GST-AICD could indeed gradually diffuse into the preformed droplets (Fig. 3*C*). The condensates are not evenly distributed, which may explain the uneven recruitment and distribution of GST-AICD (Fig. 3*C*).

Dual Modulation on Aβ42 Production by GSAP-16K. GSAP-16K was shown to activate γ-secretase activity by enhancing production of both Aβ40 and Aβ42 (16, 21). Our finding of concentration-dependent LLPS for GSAP-16K, together with direct interaction between GSAP-16K and AICD (16, 23), hints at a molecular mechanism for the regulation of APP-C99 cleavage by GSAP-16K. To uncover details of this mechanism, we systematically investigated APP cleavage by γ-secretase using the Amplified luminescent proximity homogeneous assay-linked immunosorbent assay (AlphaLISA) assay (33). In the reaction mixture, the substrate APP-C99 was supplied at a final concentration of 1 μM, ∼50-fold higher than that of the enzyme γ-secretase. The reaction was allowed to proceed for 4 h at 37 °C. AICD, generated by wild-type (WT) γ-secretase, can be detected by western blots (*SI Appendix*, Fig. S5*A*). The γ-secretase inhibitor L685,458 specifically inhibits the

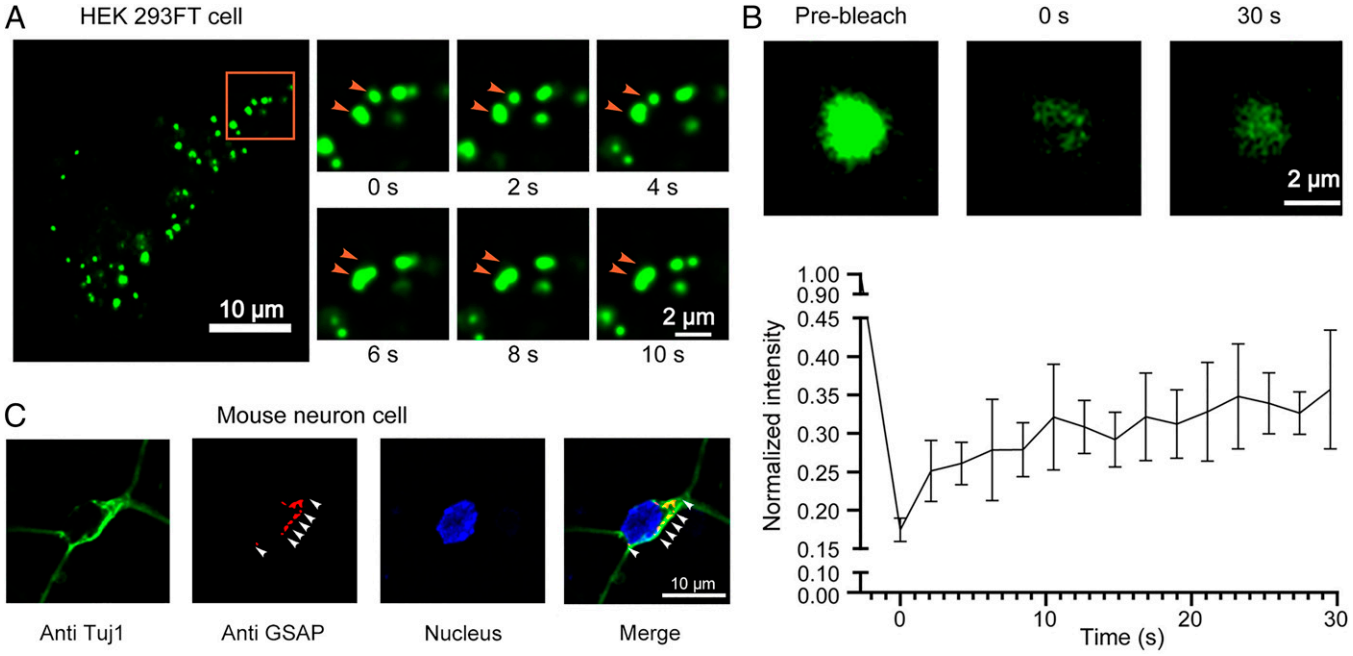

Fig. 2. GSAP-16K forms puncta-like condensates and droplets in cells. (*A*) GSAP-16K droplets display clear features of fluidity. GFP-GSAP-16K forms puncta-like condensates and droplets in HEK293FT cells (*Left*). The fluidic nature is shown by the fusion of two neighboring droplets over 10 s (*Right*). (*B*) FRAP of the GFP-GSAP-16K droplets in HEK293FT cells. Three temporal snapshots of a droplet are shown (*Upper*). Quantitative analysis, averaged for the results of FRAP on three different droplets, is shown (*Lower*). Error bar: SD. (*C*) Endogenous GSAP forms puncta-like condensates and droplets in the mouse neuronal cells. Shown here are immunofluorescence images of endogenous GSAP in the primary mouse neuronal cells. Anti-Tuj1 (β-III-Tubulin) was used as a neuronal marker. Green, Tuj1; red, GSAP. Puncta-like condensates and droplets are indicated by orange arrows. Blue, nucleus.

production of AICD (*SI Appendix*, Fig. S5). Under these conditions, less than 5% of APP-C99 could be cleaved by γ-secretase (*SI Appendix*, Fig. S5*A*).

With increasing concentrations from 0 to 4.5 μM, GSAP-16K exhibits dual modulation on the production of Aβ42 (Fig. 4*A*). In the absence of GSAP-16K, the concentration of Aβ42 reached 259 ± 8 pg/mL. With increasing concentrations of GSAP-16K up to 3 μM, the production of Aβ42 steadily increases, peaking at 1,321 ± 255 pg/mL (Fig. 4*A*). At GSAP-16K concentrations higher than 3 μM, Aβ42 production decreases precipitously, reaching a low level of about 364 ± 63 pg/mL at 4.5 μM GSAP-16K.

In contrast to Aβ42, the production of Aβ40 remains nearly unchanged in the concentration range of 0 to 3 μM GSAP-16K (Fig. 4*B*). Aβ40 production decreases markedly beyond 3 μM GSAP-16K and reached a basal value of 195 ± 43 pg/mL at 4.5 μM GSAP-16K (Fig. 4*B*). Similar to Aβ42 production (Fig. 4*A*), the combined production of Aβ42 and Aβ40 displays a bell-shaped curve with respect to the total concentration of GSAP-16K, increasing in the range from 0 to 3 μM and

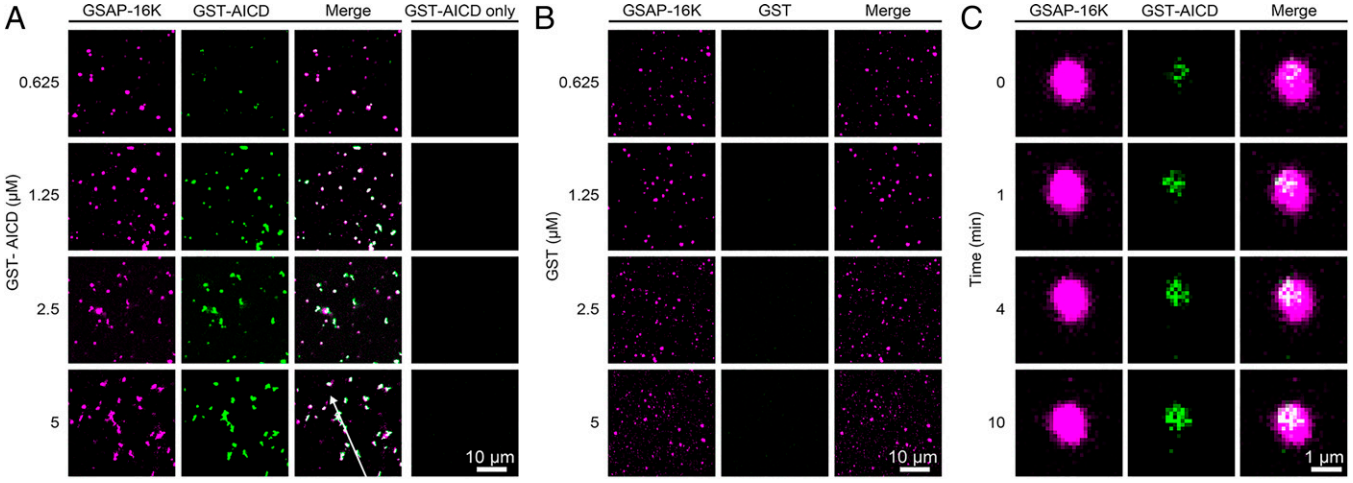

Fig. 3. AICD is incorporated into the GSAP-16K droplets in vitro. (*A*) GST-AICD colocalizes with the GSAP-16K puncta-like condensates and droplets in vitro. Alexa488-labeled GST-AICD at the indicated concentrations was incubated with 40 μM Alexa647-labeled GSAP-16K in the absence of PEG for 1 h (first three columns). The white arrow indicates the position of line scans (refer to *SI Appendix*, Fig. S4*C*). GST-AICD alone fails to form condensates/droplets (fourth column). (*B*) GST does not colocalize with GSAP-16K puncta-like condensates and droplets. (*C*) AICD can be incorporated into preformed GSAP-16K condensates/droplets. Shown here are temporal snapshots of AICD incorporation into preformed GSAP-16K droplets. The first snapshot (0 min) was taken less than 1 min after adding 5 μM AICD to the preformed GSAP-16K droplets.

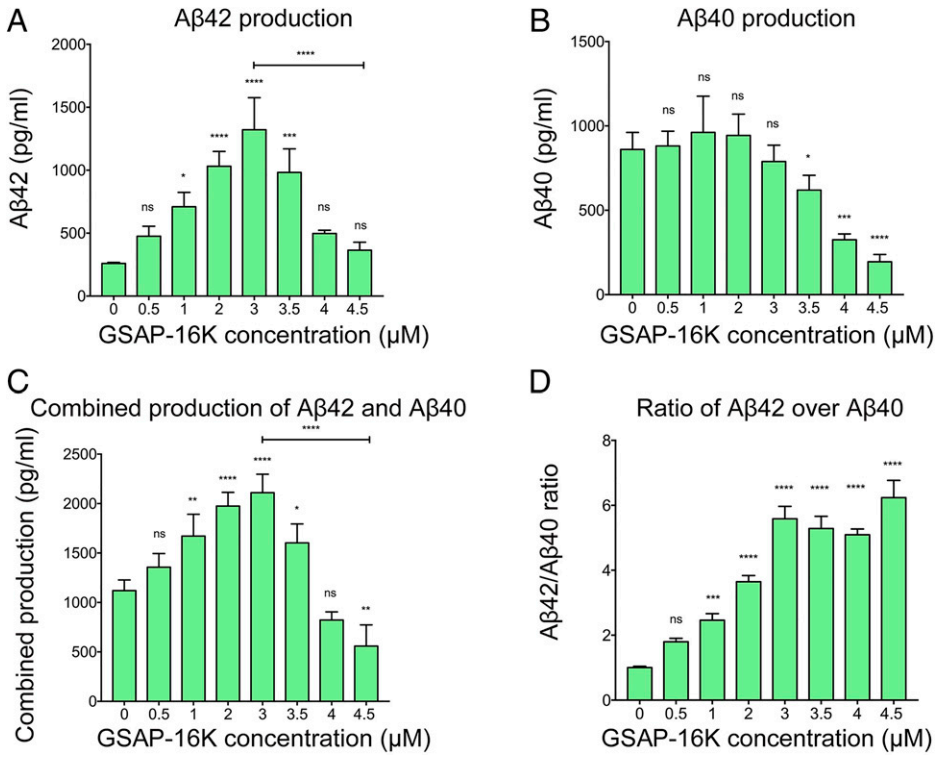

Fig. 4. Dual modulation of Aβ42 production by GSAP-16K. (*A*) GSAP-16K exhibits dual modulation on Aβ42 production. Aβ42 production peaks in the presence of 3 μM GSAP-16K. One-way ANOVA was used to analyze the statistical significance compared with that in the absence of GSAP-16K. If not specified, one-way ANOVA was applied for statistical analysis. (*B*) Aβ40 production decreases in the presence of 3 μM or more GSAP-16K. (*C*) The combined production of Aβ42 and Aβ40 exhibits a bell-shaped curve with respect to the total concentration of GSAP-16K. (*D*) The Aβ42/Aβ40 ratio is elevated proportionally in the GSAP-16K concentration range of 0 to 3 μM. Aβ40 and Aβ42 were quantified using the AlphaLISA kit (33). Each experiment was independently repeated three times. Error bar: SD. **P* < 0.05; ***P* < 0.01; ****P* < 0.001; *****P* < 0.0001; ns: no significant.

decreasing in the range from 3 to 4.5 μM (Fig. 4*C*). Most notably, as a result of the observed modulation on the production of Aβ42 and Aβ40, the Aβ42/Aβ40 ratio increases almost linearly within the increasing concentration range of 0 to 3 μM GSAP-16K and levels off in the range 3 to 4.5 μM (Fig. 4*D*).

LLPS of GSAP-16K Governs Dual Modulation. GSAP-16K at 3 μM concentration marks a turning point for its dual modulation on Aβ42 production (Fig. 4*A*) or the combined production of Aβ42 and Aβ40 (Fig. 4*C*). LLPS of GSAP-16K likely constitutes the underlying mechanism for the observed dual modulation. To investigate this scenario, we first examined the reaction mixture under a confocal microscope (*SI Appendix*, Fig. S6*A*). The puncta-like condensates/droplets appear a bit amorphous, which might be related to the detergents and lipids in the assay system. With increasing concentrations of GSAP-16K, the percentages of the area occupied by condensates/droplets steadily increase (*SI Appendix*, Fig. S6*B*). Alexa647-labeled GSAP-16K and Alexa488-labeled APP-C99 colocalize in these puncta-like condensates/droplets (*SI Appendix*, Fig. S6*A*). This is also validated by line scans of the images of Alexa647-labeled GSAP-16K, Alexa488-labeled APP-C99, and blue fluorescence protein (BFP)–tagged γ-secretase (*SI Appendix*, Fig. S6*C*).

We next centrifuged the reaction mixture and used western blots to examine the target proteins in the supernatant (Fig. 5*A*) and in the pellet (Fig. 5*B*). The pellet contains condensates/droplets. These experiments were repeated three times, allowing quantification of the target protein amount (Fig. 5 *C*–*F*). In the total concentration range of 0.5 to 4.5 μM, the amount of GSAP-16K in the supernatant (GSAP-16K in the dilute phase) increases steadily up to 3 μM but decreases sharply afterward (Fig. 5 *A* and *C*). In contrast, GSAP-16K in the pellet begins to significantly accumulate at 2 μM and steadily increases afterward (Fig. 5 *B* and *D*).

The amount of the substrate APP-C99 in the supernatant (APP-C99 in dilute phase) gradually decreases with increasing amounts of GSAP-16K (Fig. 5*E*). Compared with that in the absence of GSAP-16K, the amount of APP-C99 in dilute phase is reduced by ∼82.4% in the presence of 4.5 μM GSAP-16K. In contrast, the amount of APP-C99 in the pellet steadily increases (Fig. 5*F*), approximately proportional to the amount of GSAP-16K in the pellet. Because APP-C99 remains barely detectable in the pellet in the absence of GSAP-16K, it is safe to conclude that APP-C99 was brought into the condensates by GSAP-16K.

The amount of GSAP-16K in dilute phase roughly correlates with Aβ42 production, both displaying a bell-shaped curve (Figs. 4*A* and 5*C*). An explanation is that, GSAP-16K in dilute phase delivers APP-C99 to the active site of γ-secretase for increased production of Aβ42, and GSAP-16K in the condensates sequesters APP-C99, making it inaccessible to γ-secretase.

This explanation is based on the assumption that γ-secretase should remain in the supernatant and not be incorporated into these condensates/droplets. This is indeed true, as Pen-2, one of the γ-secretase components, remains entirely in the supernatant at the end of the reaction (Fig. 5*A*). In addition, the marked reduction of APP-C99 in dilute phase in the presence of higher concentrations of GSAP-16K is not mainly due to proteolytic consumption because only a very small fraction of the substrate had been cleaved by γ-secretase (*SI Appendix*, Fig. S5*A*). Consistent with this analysis, similar results were obtained when WT γ-secretase was replaced by the catalytic mutant PS1-D385A (*SI Appendix*, Fig. S7).

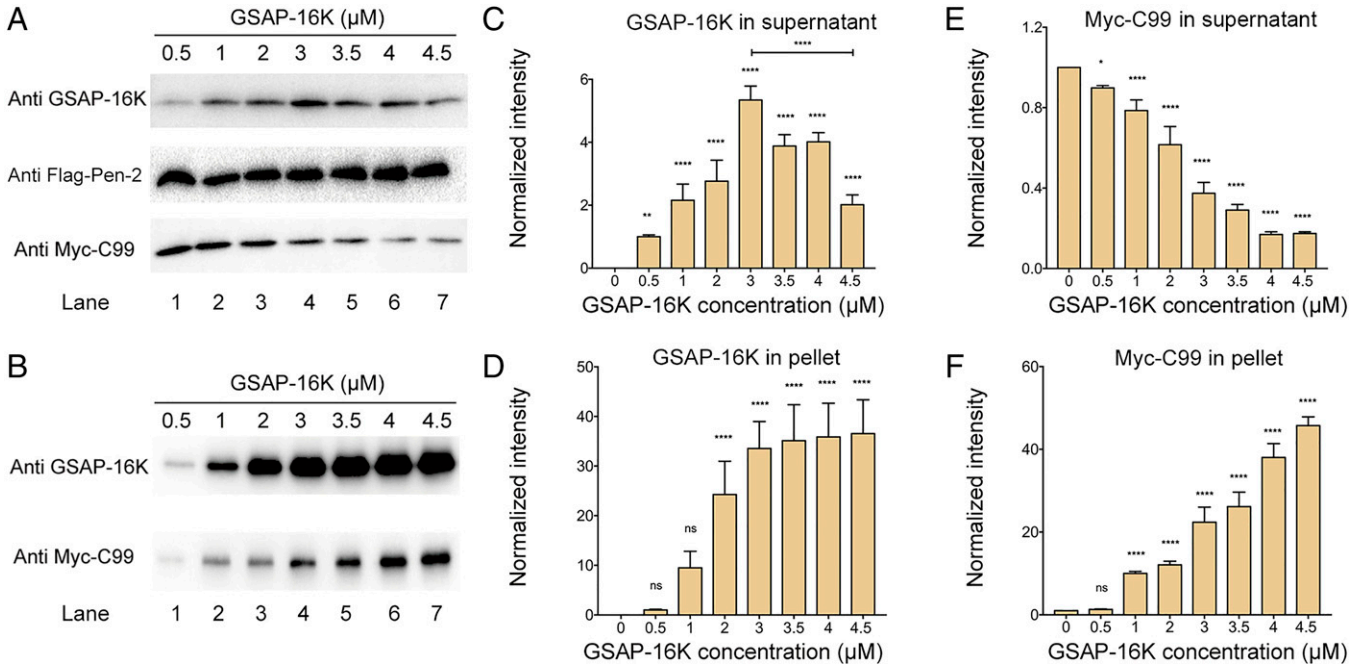

Fig. 5. The amount of APP-C99 in dilute phase was controlled by GSAP-16K. (*A*) The amount of GSAP-16K in dilute phase reaches a peak value at 3 μM. Shown here are results of western blots of GSAP-16K, Pen-2, and APP-C99 in the supernatant of the reaction mixture. Following 4 h of γ-secretase cleavage, the reaction mixture was centrifuged to separate the supernatant from the pellet. The pellet contains GSAP-16K condensates/droplets. (*B*) The amounts of both GSAP-16K and APP-C99 in the pellet grow with increasing total concentrations of GSAP-16K. Shown here are results of western blots of GSAP-16K and APP-C99 in the pellet of the reaction mixture. (*C*) The amount of GSAP-16K in dilute phase displays a bell-shaped curve with respect to the total GSAP-16K concentration range of 0 to 4.5 μM. Shown here (and in *D*–*F*) are the averaged results of three independent experiments. Error bar: SD. (*D*) The amount of GSAP-16K in the pellet increases steadily in the presence of increasing concentrations of GSAP-16K. (*E*) The amount of APP-C99 in dilute phase steadily decreases with increasing total concentrations of GSAP-16K. (*F*) The amount of APP-C99 in the pellet grows steadily with increasing total concentrations of GSAP-16K. *$P < 0.05$; **$P < 0.01$; ****$P < 0.0001$; ns: no significant.

A Working Model of γ-Secretase Modulation by GSAP-16K. Our experiments reveal dual modulation on Aβ42 production by GSAP-16K. GSAP-16K in dilute phase enhances the proteolytic production of Aβ42, whereas formation of the GSAP-16K condensates suppresses Aβ42 production by sequestering the substrate APP-C99 in the condensates. LLPS—the molecular basis of the dual modulation—strictly depends on physical interactions between GSAP-16K and AICD (16, 23). To better understand the mechanism, we examined various fragments of AICD and identified a nine-residue fragment (residues 730 to 738; GST-APP 730 to 738) that interacts with GSAP-16K. Similar efforts led to the identification of a 25-residue fragment (residues 734 to 758; His-GSAP-16K 734 to 758) of GSAP-16K that binds AICD.

Using purified recombinant proteins, we show that GST-APP 730 to 738 forms a stable complex with His-GSAP-16K 734 to 758 on gel filtration (Fig. 6*A*). Using western blots, we demonstrate that Flag-tagged GST-APP 730 to 738 and His-tagged GSAP-16K 734 to 758 are both expressed in cells and stably interact with each other (*SI Appendix*, Fig. S8*A*). Confirming specific interactions, deletion of 25 residues in GSAP-16K (GSAP-16K Δ734 to 758) results in disruption of the interaction and colocalization between APP-C99 and GSAP-16K (*SI Appendix*, Fig. S8 *B* and *C*).

Notably, the AICD fragment responsible for binding GSAP-16K is located only five residues downstream of the APP-C99 sequence that forms the induced β-strand (34) (Fig. 6*B*). The induced β-strand guides the substrate into the active site of PS1, an essential step in γ-secretase cleavage (14, 34–36). In the cryo-electron microscopy (cryo-EM) structure of γ-secretase bound to an APP-C99 fragment, the sequences downstream of the induced β-strand lack defined structure, indicating high flexibility (34). This analysis suggests that GSAP-16K may facilitate recruitment of APP-C99 into the active site of PS1 by promoting formation of the induced β-strand through direct interaction with its downstream sequences (Fig. 6*C*).

In this working model, GSAP-16K in dilute phase uses its 25-residue fragment to interact with the 9-residue AICD fragment of APP-C99 (Fig. 6*C*). This interaction presumably facilitates formation of the induced β-strand, thus assisting recruitment of APP-C99 into γ-secretase in a defined fashion and consequently, enhancing Aβ42 production. However, at higher concentrations, GSAP-16K forms puncta-like condensates and droplets, which trap the substrate APP-C99 away from γ-secretase, thus suppressing cleavage of APP-C99 (Fig. 6*C*).

Discussion

Aβ42 originates from Aβ48, and Aβ48 is due to the endopeptidase activity of γ-secretase on APP-C99 (37). Similarly, Aβ40 originates from Aβ49. Neither Aβ48 nor Aβ49 interacts with GSAP-16K. Therefore, dual modulation of Aβ42 production is achieved through the first cleavage of APP-C99 by γ-secretase. Why does GSAP-16K binding to APP-C99 preferentially facilitate the production of Aβ48 but not Aβ49? One likely answer is that, due to steric hindrance, binding by GSAP-16K favors formation of the induced β-strand by residues 721 to 724 as opposed to residues 722 to 725 of APP-C99. This arrangement, which generates Aβ48, leaves one extra amino acid between the induced β-strand and the GSAP-16K binding fragment. Another possibility is that GSAP-16K may induce conformational changes in PS1 that, in turn, facilitate Aβ48 production (21). However, this possibility suffers from the unanswered question of why such changes in PS1

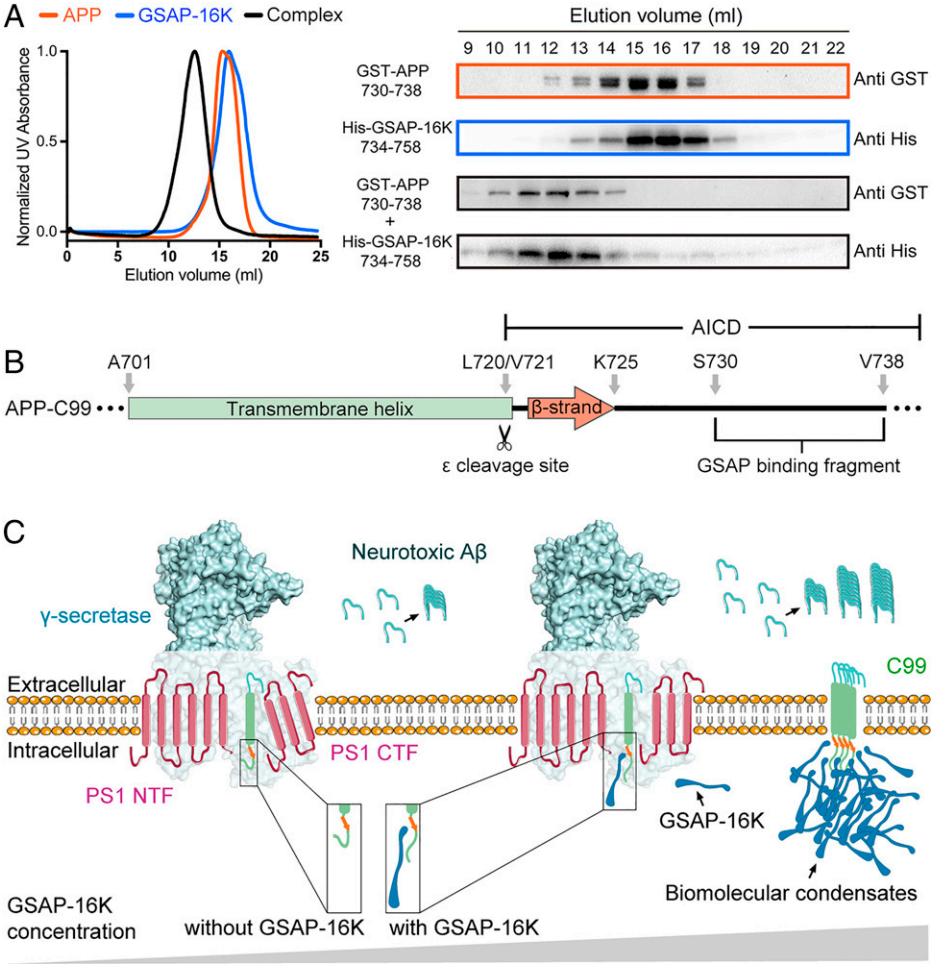

Fig. 6. A working model of γ-secretase modulation by GSAP-16K. (*A*) GSAP-16K (residues 734 to 758) and AICD (residues 730 to 738) form a stable complex. Shown here are representative chromatographs of gel filtration (*Left*) and western blots of the indicated fractions from gel filtration (*Right*). UV, ultraviolet. (*B*) The AICD fragment that binds GSAP-16K is located five residues downstream of the induced β-strand from APP-C99. Cleavage between Leu720 and Val721 of APP-C99 by γ-secretase generates Aβ49 (Asp672 through Leu720) and AICD (Val721 through Asn770). (*C*) A mechanistic model of γ-secretase modulation by GSAP-16K through LLPS. In the absence of GSAP-16K, the recruitment of APP-C99 into γ-secretase favors the production of Aβ49, which is successively processed into Aβ40. GSAP-16K in dilute phase promotes the production of Aβ48, which is processed into Aβ42 (21). GSAP-16K condensates, and droplets sequester APP-C99, making the substrate inaccessible to γ-secretase. PS1 CTF: PS1 C-terminal fragment; PS1 NTF: PS1 N-terminal fragment.

would have no impact on the cleavage of other substrates of γ-secretase. In addition, despite repeated efforts, we have been unable to detect direct interactions between GSAP-16K and γ-secretase.

Due to their fluidity and mobile nature, the condensates/droplets of GSAP-16K and APP-C99 may serve as a dynamic protein pool for the regulation of the availability of APP-C99 for γ-secretase cleavage. Consistent with this analysis, GSAP was shown to regulate APP trafficking (38). In live cells, APP vesicles can be classified into mobile and immobile particles; GSAP knockdown reduces immobile APP vesicles (38).

LLPS requires a critical concentration. The amounts of GSAP-16K in the pellet remain relatively low at or below 1 μM GSAP-16K but sharply increase at or above 2 μM GSAP-16K (Fig. 5*D*). In the patient brain, the level of GSAP expression was found to be elevated, and GSAP-16K existed in an aggregated state (17, 19). These observations suggest that aggregated GSAP-16K as a result of elevated concentrations may contribute to the pathological state of AD (39, 40). In fact, GSAP in mouse neuronal cells readily formed puncta-like condensates (Fig. 2*C*). The spatiotemporal and biphasic regulation of GSAP-16K in human may contribute to the development of AD.

The expression levels of GSAP were found to correlate with AD susceptibility (17). This observation is consistent with our finding that increased GSAP concentrations result in an elevated Aβ42/Aβ40 ratio, which is thought to contribute to AD genesis. At GSAP-16K concentrations higher than 3 μM, the combined production of Aβ42 and Aβ40 is markedly decreased in the in vitro cleavage assay (Fig. 4*C*), but the Aβ42/Aβ40 ratio remains high (Fig. 4*D*). Intriguingly, the vast majority of AD-derived mutations in PS1 result in reduction of γ-secretase activity but elevation of the Aβ42/Aβ40 ratio (33). Despite these tantalizing clues, the GSAP-16K concentration in patient brain remains to be determined.

Abnormal protein aggregation is a recurring theme in neurodegenerative diseases (39, 41). In addition to amyloid plaques, neurofibrillary tangles constitute another hallmark of AD. The primary constituent of neurofibrillary tangles is the hyperphosphorylated Tau protein (42, 43). Tau forms droplets in vitro and in vivo to initiate protein aggregation (44–46). In addition to Tau, FUS (47–49), TDP-43 (50), hnRNPA1 (51, 52), C9orf72 (53), and α-synuclein (54), each implicated in a neurodegenerative disease, undergo LLPS (55). Our finding of LLPS by GSAP-16K and its dual modulation on γ-secretase activity represents an important expansion on the biological

impact of LLPS and suggests potential strategies for reducing Aβ42/Aβ40 ratios in AD patients.

LLPS is mediated by the multivalency of biomolecules of two types, either with modular domains or with intrinsically disordered regions (56). GSAP-16K likely contains both structural core domains (*SI Appendix*, Fig. S1) and intrinsically disordered sequences as predicted by the online software MetaDisorder (https://predictprotein.org). Additional study is needed to assess what sequence elements of GSAP-16K mediate the LLPS.

Inhibition of γ-secretase activity toward APP cleavage represents an attractive strategy for AD intervention. Small-molecule inhibitors and modulators have been developed to target γ-secretase. Unfortunately, none of these inhibitors have demonstrated cognitive improvements in clinical trials, largely due to side effects associated with cleavage inhibition of substrates other than APP (57–59). These failed efforts force scientists to look for protein targets that specifically regulate APP cleavage by γ-secretase. Along this line, several proteins have been identified to specifically regulate Aβ production; these include GSAP-16K (16), Hif-1α (60), IFITM3 (61), and SERP1 (62). Our study constitutes a clearly documented example of how such proteins may mechanistically regulate γ-secretase activity. Because GSAP-16K enhances the Aβ42/Aβ40 ratio through its interaction with APP-C99, breaking up this interaction via small molecules may markedly reduce the Aβ42/Aβ40 ratio, presumably reducing formation of the β-amyloid plaques in patients. Such molecules should only modulate APP cleavage and have little impact on other substrates of γ-secretase.

Materials and Methods

Molecular Cloning. The GSAP-16K complementary DNA (cDNA) was a gift from the laboratory of Paul Greengard (16). GSAP-16K cDNA was subcloned into pET21b for recombinant expression and the pLJMGFP vector for stable cell line generation. For the in vitro fusion assay, the cDNA sequences for AICD (residues 721 to 770) with an N-terminal GST and a C-terminal Myc tag were subcloned into the pQlink expression vector. The cDNA for PS1-NTF with an N-terminal BFP was subcloned into the pMlink vector to generate BFP-PS1–containing γ-secretase (36).

Protein Expression and Purification. All constructs in pET21b were expressed in *E. coli* BL21 (DE3). APP-C99 and γ-secretase were expressed and purified as described (36).

Microscopy. A NIKON A1 RMP microscope was used for imaging. The images were analyzed using NIS-Elements AR Analysis and NIS-Elements Viewer 5.21.

In Vitro LLPS/Condensates Formation Assay. The GSAP-16K protein was labeled using the fluorescent dye Alexa647 carboxylic acid (succinimidyl ester) (ThermoFisher). After removal of the free dye, the labeled GSAP-16K was incubated in an assay buffer at room temperature for 1 h before imaging. The Alexa labeling efficiency is nearly 1%.

FRAP. In FRAP experiments in solution, the selected droplets were bleached using a 638-nm laser pulse, and the recovery was recorded for 15 min after bleaching. For FRAP experiments in cells, the puncta-like droplets were bleached using a 488-nm laser pulse, and the recovery was recorded for 30 s.

Cell Culture and Generation of Stable Cell Lines. To generate a cell line that stably expresses GFP or GFP-GSAP-16K, the specific pLJMGFP vector and two helper plasmids (pCMV-VSVG and psPAX2) were transfected into HEK293FT cells for lentivirus generation. Puromycin-resistant cells were selected as the stable cell line.

Immunofluorescence Staining. The cortical neuronal cells from a P0 C57BL/6J mouse were fixed. Following incubation with anti-GSAP antibodies (Abcam; ab106630 against C-terminal sequences of GSAP or Novus Biologicals; NBP1-78400 against N-terminal sequences of GSAP) and anti–β-Tubulin (Tuj1) antibodies, the neuronal cells were incubated with goat anti-rabbit antibodies and goat anti-mouse antibodies. The cells were then washed using phosphate buffered saline (PBS) and stained using the dye Hoechst 33258 before imaging by microscope.

In Vitro γ-Secretase Cleavage Assay. The assay was performed as described (33). The reaction mixture was centrifuged at 12,000 × *g* for 1 h to separate the droplets/condensates from the supernatant.

Western Blots. Protein samples resolved by sodium dodecyl sulfate–polyacrylamide gel electrophoresis (SDS-PAGE) were transferred to a polyvinylidene fluoride (PVDF) membrane using the semidry transfer method. The membrane was blocked prior to incubation with the primary and secondary antibodies. The chemiluminescence reagent (ThermoFisher) was used to visualize the results.

Quantification and Statistical Analysis. Statistical analysis was carried out using Excel, GraphPad Prism, ImageJ, and NIS-Elements AR Analysis. Data are presented as the mean ± SD.

Comigration Assay. GST-APP 730 to 738 and His8-tagged GSAP-16K 734 to 758 were cotransformed into *E. coli* (DH5a) and cultured at 37 °C until OD (optical density) = 0.8 at 600 nm. The cell culture was shifted to 20 °C, and 200 mM isopropyl-beta-D-thiogalactopyranoside was added to the culture at a final concentration of 200 μM. Following overnight culture, the cells were harvested and resuspended in the buffer 25 mM Trizma base, pH 8.0, 150 mM NaCl, and 1 mM phenylmethylsulfonyl fluoride. For purification, the supernatant after centrifugation (13,000 × *g*, 1 h) was first loaded on the Ni-NTA column. The eluate from the nickel nitrilotriacetic acid column was applied to the glutathione sepharose 4B resin (GS4B) column. GST-APP 730 to 738 alone was purified by the GS4B column, and His8-GSAP-16K 734 to 758 alone was purified by the Ni-NTA column. The final elution was applied to gel filtration. The fractions were detected by western blot.

CD Spectra. GSAP-16K concentration was adjusted to 0.2 mg/mL. The CD spectra were collected in a 1-mm cuvette under the wavelength from 195 to 260 nm on a Chirascan Plus (Applied Photophysics) spectropolarimeter. The temperature range was set from 25 °C to 94 °C, with a step size of 3 °C. The data were processed by Pro-Data Viewer.

Limited Proteolysis. GSAP-16K at 0.25 mg/mL was digested with varying concentrations of Proteinase K or V8 Protease. For each protease, threefold serial dilution was used to generate a concentration gradient. The reactions were carried out for 10 min at room temperature and stopped by the addition of 10 mM PMSF. An aliquot of each reaction was analyzed by SDS-PAGE.

Data Availability. All study data are included in the article and/or supporting information.

ACKNOWLEDGMENTS. We thank the School of Life Sciences, Tsinghua University–Nikon Biological Imaging Center (Tsinghua University) for technical assistance, Dr. Yichang Jia and Dr. Xue Zhang for guidance in preparation of the stable cell lines and staining of the mouse neuronal cells, and Cuiyan Zhou at the Tsinghua University Branch of the China National Center for Protein Sciences for help. This work was supported by the National Key R&D Program of China (grant: 2020YFA0509300), the Ministry of Science and Technology of China, the National Natural Science Foundation of China (grant: 81920108015 and 31930059), and the Key R&D Program of Zhejiang Province (grant: 2020C04001). R.Z. is supported by a fellowship from the Beijing Advanced Innovation Center for Structural Biology.

Author affiliations: [a]Beijing Advanced Innovation Center for Structural Biology, Beijing Frontier Research Center for Biological Structure, Tsinghua–Peking Joint Center for Life Sciences, School of Life Sciences, Tsinghua University, Beijing 100084, China; [b]State Key Laboratory for Agrobiotechnology, College of Biological Sciences, China Agricultural University, Beijing 100193, China; [c]Laboratory of Molecular and Cellular Neuroscience, The Rockefeller University, New York, NY, 10065; [d]Westlake Laboratory of Life Science and Biomedicine, Westlake Institute for Advanced Study, Hangzhou 310024, China; [e]Key Laboratory of Structural Biology of Zhejiang Province, School of Life Sciences, Westlake University, Hangzhou 310024, China; and [f]Institute of Biology, Westlake Institute for Advanced Study, Hangzhou 310024, China

1. M. Kidd, Alzheimer's disease: An electron microscopical study. *Brain* **87**, 307–320 (1964).
2. A. Alzheimer, About a peculiar disease of the cerebral cortex. *Centralblatt Nervenheilkunde Psychiatrie* **30**, 177–179 (1907).
3. D. J. Selkoe, Alzheimer's disease: Genes, proteins, and therapy. *Physiol. Rev.* **81**, 741–766 (2001).
4. D. J. Selkoe, J. Hardy, The amyloid hypothesis of Alzheimer's disease at 25 years. *EMBO Mol. Med.* **8**, 595–608 (2016).
5. T. E. Golde, S. Estus, L. H. Younkin, D. J. Selkoe, S. G. Younkin, Processing of the amyloid protein precursor to potentially amyloidogenic derivatives. *Science* **255**, 728–730 (1992).
6. F. S. Esch *et al.*, Cleavage of amyloid beta peptide during constitutive processing of its precursor. *Science* **248**, 1122–1124 (1990).
7. R. Vassar *et al.*, Beta-secretase cleavage of Alzheimer's amyloid precursor protein by the transmembrane aspartic protease BACE. *Science* **286**, 735–741 (1999).
8. C. Haass, D. J. Selkoe, Cellular processing of beta-amyloid precursor protein and the genesis of amyloid beta-peptide. *Cell* **75**, 1039–1042 (1993).
9. T. Sato *et al.*, Active gamma-secretase complexes contain only one of each component. *J. Biol. Chem.* **282**, 33985–33993 (2007).
10. B. De Strooper, Aph-1, Pen-2, and Nicastrin with Presenilin generate an active gamma-Secretase complex. *Neuron* **38**, 9–12 (2003).
11. J. A. Hardy, G. A. Higgins, Alzheimer's disease: The amyloid cascade hypothesis. *Science* **256**, 184–185 (1992).
12. H. F. Dovey *et al.*, Functional gamma-secretase inhibitors reduce beta-amyloid peptide levels in brain. *J. Neurochem.* **76**, 173–181 (2001).
13. A. Haapasalo, D. M. Kovacs, The many substrates of presenilin/γ-secretase. *J. Alzheimers Dis.* **25**, 3–28 (2011).
14. G. Yang *et al.*, Structural basis of γ-secretase inhibition and modulation by small molecule drugs. *Cell* **184**, 521–533.e14 (2021).
15. E. Wong, G. R. Frost, Y. M. Li, γ-Secretase modulatory proteins: The guiding hand behind the running scissors. *Front. Aging Neurosci.* **12**, 614690 (2020).
16. G. He *et al.*, Gamma-secretase activating protein is a therapeutic target for Alzheimer's disease. *Nature* **467**, 95–98 (2010).
17. M. Zhu *et al.*, Common GSAP promoter variant contributes to Alzheimer's disease liability. *Neurobiol. Aging* **35**, 2656.e1–2656.e7 (2014).
18. P. Xu *et al.*, GSAP regulates lipid homeostasis and mitochondrial function associated with Alzheimer's disease. *J. Exp. Med.* **218**, e20202446 (2021).
19. J. Satoh, H. Tabunoki, T. Ishida, Y. Saito, K. Arima, Immunohistochemical characterization of γ-secretase activating protein expression in Alzheimer's disease brains. *Neuropathol. Appl. Neurobiol.* **38**, 132–141 (2012).
20. J. Chu, E. Lauretti, C. P. Craige, D. Praticò, Pharmacological modulation of GSAP reduces amyloid-β levels and tau phosphorylation in a mouse model of Alzheimer's disease with plaques and tangles. *J. Alzheimers Dis.* **41**, 729–737 (2014).
21. E. Wong *et al.*, GSAP modulates γ-secretase specificity by inducing conformational change in PS1. *Proc. Natl. Acad. Sci. U.S.A.* **116**, 6385–6390 (2019).
22. S. N. Hajjari *et al.*, MicroRNA-4422-5p as a negative regulator of amyloidogenic secretases: A potential biomarker for Alzheimer's disease. *Neuroscience* **463**, 108–115 (2021).
23. D. Angira, R. Chikhale, K. Mehta, R. A. Bryce, V. Thiruvenkatam, Tracing the GSAP-APP C-99 interaction site in the β-amyloid pathway leading to Alzheimer's disease. *ACS Chem. Neurosci.* **10**, 3868–3879 (2019).
24. C. L. Deatherage, A. Hadziselimovic, C. R. Sanders, Purification and characterization of the human γ-secretase activating protein. *Biochemistry* **51**, 5153–5159 (2012).
25. S. Boeynaems *et al.*, Protein phase separation: A new phase in cell biology. *Trends Cell Biol.* **28**, 420–435 (2018).
26. S. Alberti, A. Gladfelter, T. Mittag, Considerations and challenges in studying liquid-liquid phase separation and biomolecular condensates. *Cell* **176**, 419–434 (2019).
27. C. P. Brangwynne *et al.*, Germline P granules are liquid droplets that localize by controlled dissolution/condensation. *Science* **324**, 1729–1732 (2009).
28. P. Li *et al.*, Phase transitions in the assembly of multivalent signalling proteins. *Nature* **483**, 336–340 (2012).
29. T. J. Nott *et al.*, Phase transition of a disordered nuage protein generates environmentally responsive membraneless organelles. *Mol. Cell* **57**, 936–947 (2015).
30. X. Su *et al.*, Phase separation of signaling molecules promotes T cell receptor signal transduction. *Science* **352**, 595–599 (2016).
31. M. Zeng *et al.*, Reconstituted postsynaptic density as a molecular platform for understanding synapse formation and plasticity. *Cell* **174**, 1172–1187.e16 (2018).
32. O. Annunziata *et al.*, Effect of polyethylene glycol on the liquid-liquid phase transition in aqueous protein solutions. *Proc. Natl. Acad. Sci. U.S.A.* **99**, 14165–14170 (2002).
33. L. Sun, R. Zhou, G. Yang, Y. Shi, Analysis of 138 pathogenic mutations in presenilin-1 on the in vitro production of Aβ42 and Aβ40 peptides by γ-secretase. *Proc. Natl. Acad. Sci. U.S.A.* **114**, E476–E485 (2017).
34. R. Zhou *et al.*, Recognition of the amyloid precursor protein by human γ-secretase. *Science* **363**, eaaw0930 (2019).
35. G. Yang *et al.*, Structural basis of Notch recognition by human γ-secretase. *Nature* **565**, 192–197 (2019).
36. P. Lu *et al.*, Three-dimensional structure of human γ-secretase. *Nature* **512**, 166–170 (2014).
37. M. Takami *et al.*, Gamma-secretase: Successive tripeptide and tetrapeptide release from the transmembrane domain of beta-carboxyl terminal fragment. *J. Neurosci.* **29**, 13042–13052 (2009).
38. J. C. Chang *et al.*, GSAP regulates amyloid beta production through modulation of amyloid precursor protein trafficking. bioRxiv [Preprint]. https://doi.org/10.1101/2020.11.12.379313 (12 November 2020).
39. F. Chiti, C. M. Dobson, Protein misfolding, functional amyloid, and human disease. *Annu. Rev. Biochem.* **75**, 333–366 (2006).
40. A. Aguzzi, T. O'Connor, Protein aggregation diseases: Pathogenicity and therapeutic perspectives. *Nat. Rev. Drug Discov.* **9**, 237–248 (2010).
41. C. Mathieu, R. V. Pappu, J. P. Taylor, Beyond aggregation: Pathological phase transitions in neurodegenerative disease. *Science* **370**, 56–60 (2020).
42. I. Grundke-Iqbal *et al.*, Abnormal phosphorylation of the microtubule-associated protein tau (tau) in Alzheimer cytoskeletal pathology. *Proc. Natl. Acad. Sci. U.S.A.* **83**, 4913–4917 (1986).
43. D. W. Cleveland, S. Y. Hwo, M. W. Kirschner, Physical and chemical properties of purified tau factor and the role of tau in microtubule assembly. *J. Mol. Biol.* **116**, 227–247 (1977).
44. S. Ambadipudi, J. Biernat, D. Riedel, E. Mandelkow, M. Zweckstetter, Liquid-liquid phase separation of the microtubule-binding repeats of the Alzheimer-related protein Tau. *Nat. Commun.* **8**, 275 (2017).
45. X. Zhang *et al.*, RNA stores tau reversibly in complex coacervates. *PLoS Biol.* **15**, e2002183 (2017).
46. S. Wegmann *et al.*, Tau protein liquid-liquid phase separation can initiate tau aggregation. *EMBO J.* **37**, e98049 (2018).
47. A. Patel *et al.*, A liquid-to-solid phase transition of the ALS protein FUS accelerated by disease mutation. *Cell* **162**, 1066–1077 (2015).
48. K. A. Burke, A. M. Janke, C. L. Rhine, N. L. Fawzi, Residue-by-residue view of in vitro FUS granules that bind the C-terminal domain of RNA polymerase II. *Mol. Cell* **60**, 231–241 (2015).
49. T. Murakami *et al.*, ALS/FTD mutation-induced phase transition of FUS liquid droplets and reversible hydrogels into irreversible hydrogels impairs RNP granule function. *Neuron* **88**, 678–690 (2015).
50. A. E. Conicella, G. H. Zerze, J. Mittal, N. L. Fawzi, ALS mutations disrupt phase separation mediated by α-helical structure in the TDP-43 low-complexity C-terminal domain. *Structure* **24**, 1537–1549 (2016).
51. A. Molliex *et al.*, Phase separation by low complexity domains promotes stress granule assembly and drives pathological fibrillization. *Cell* **163**, 123–133 (2015).
52. Y. Lin, D. S. Protter, M. K. Rosen, R. Parker, Formation and maturation of phase-separated liquid droplets by RNA-binding proteins. *Mol. Cell* **60**, 208–219 (2015).
53. S. Boeynaems *et al.*, Phase separation of C9orf72 dipeptide repeats perturbs stress granule dynamics. *Mol. Cell* **65**, 1044–1055.e5 (2017).
54. S. Ray *et al.*, α-Synuclein aggregation nucleates through liquid-liquid phase separation. *Nat. Chem.* **12**, 705–716 (2020).
55. S. Elbaum-Garfinkle, Matter over mind: Liquid phase separation and neurodegeneration. *J. Biol. Chem.* **294**, 7160–7168 (2019).
56. S. F. Banani, H. O. Lee, A. A. Hyman, M. K. Rosen, Biomolecular condensates: Organizers of cellular biochemistry. *Nat. Rev. Mol. Cell Biol.* **18**, 285–298 (2017).
57. B. De Strooper, Lessons from a failed γ-secretase Alzheimer trial. *Cell* **159**, 721–726 (2014).
58. R. S. Doody *et al.*; Alzheimer's Disease Cooperative Study Steering Committee; Semagacestat Study Group, A phase 3 trial of semagacestat for treatment of Alzheimer's disease. *N. Engl. J. Med.* **369**, 341–350 (2013).
59. V. Coric *et al.*, Targeting prodromal Alzheimer disease with avagacestat: A randomized clinical trial. *JAMA Neurol.* **72**, 1324–1333 (2015).
60. J. C. Villa *et al.*, Nontranscriptional role of Hif-1α in activation of γ-secretase and notch signaling in breast cancer. *Cell Rep.* **8**, 1077–1092 (2014).
61. J. Y. Hur *et al.*, The innate immunity protein IFITM3 modulates γ-secretase in Alzheimer's disease. *Nature* **586**, 735–740 (2020).
62. S. Jung *et al.*, SERP1 is an assembly regulator of γ-secretase in metabolic stress conditions. *Sci. Signal.* **13**, eaax8949 (2020).